Uniform Concentric Circular Arrays With Frequency-Invariant Characteristics—Theory, Design, Adaptive Beamforming and DOA Estimation

S. C. Chan, *Member, IEEE*, and H. H. Chen, *Student Member*

***Abstract*—This paper proposes a new digital beamformer for uniform concentric circular arrays (UCCAs) having nearly frequency-invariant (FI) characteristics. The basic principle is to transform the received signals to the phase mode and remove the frequency dependency of the individual phase mode through the use of a digital beamforming or compensation network. As a result, the far-field pattern of the array, which is governed by a set of variable beamformer weights, is electronically steerable, and it is approximately invariant over a wider range of frequencies than conventional uniform circular arrays (UCAs). This also makes it possible to design the compensation network and the beamformer weights separately. The design of the compensation network is formulated as a second order cone programming (SOCP) problem and is solved optimally for minimax criterion. By employing the beamspace approach using the outputs of a set of fixed UCCA frequency-invariant beamformers (FIBs), a new beamspace MUSIC algorithm is proposed for estimating the direction-of-arrivals (DOAs) of broadband sources. Since the beampatterns of the UCCA-FIB is approximately invariant with frequency and is governed by a small set of weights, a very efficient adaptive beamformer using the minimum variance beamforming (MVB) approach can be developed. Simulation results using broadband Gaussian and multisinusoidal inputs show that the proposed adaptive UCCA-FIB is numerically better conditioned than the conventional broadband tapped-delay-line-based adaptive beamformers, due to the FI property and significantly fewer numbers of adaptive parameters. Consequently, a higher output signal-to-inference-plus-noise ratio over the conventional tapped-delay-line approach is observed. The usefulness of the proposed UCCA-FIB in broadband DOA estimation is also verified by computer simulation.**

***Index Terms*—Array processing, beamspace, broadband adaptive beamforming, broadband direction-of-arrival (DOA) estimation, design method, frequency invariant (FI), uniform concentric circular array (UCCA).**

I. Introduction

BEAMFORMING using sensor arrays is an effective method for suppressing interference whose angles of arrival are different from the desired looking direction. They find important applications in radio communications, sonar, radar, and acoustics [1]–[3]. Traditional adaptive broadband beamformer usually employs tapped-delay lines or linear transversal filters with adaptive coefficients to generate appropriate beam patterns for suppressing undesirable interference. Since the response of the array is frequency dependent, the number of coefficients of the tapped-delay lines required will increase with the signal bandwidth. In broadband adaptive beamforming, a considerable number of adaptive coefficients will be required, and it translates into increased convergence time, degraded numerical properties, and high implementation complexity. To overcome this problem, subband decomposition technique, partial adaptation, and frequency-invariant beamformers (FIBs) [4]–[8] have been proposed to reduce either the frequency band to be adapted or length of the adaptive transversal filters. In FIB, a fixed beamforming network is used to compensate for the frequency dependency of the array and generate beam patterns that are approximately invariant over the frequency band of interest, hence the name *frequency-invariant beamformers*. There are several techniques for designing FIBs with fixed beampatterns. In [6], the array aperture is discretized to obtain FIB with fixed beampatterns using the scale-frequency relationship of an array aperture. The design and implementation of such FIBs for linear arrays have been reported in [7]. Because of the discretization process, the positions of the sensors are usually nonuniform. In [4], it is observed that the design of FIBs for uniform linear arrays (ULA) is equivalent to the design of a two-dimensional (2-D) fan filter with different orientations. Using a set of fixed FIBs which covers different spatial angles of a ULA, broadband directional interference can be suppressed using a generalized sidelobe canceller (GSC)-based [9] adaptive beamformer with very few number of adaptive filter coefficients [5] (one coefficient for each beam). Moreover, compared with a traditional broadband Griffiths and Jim (GJ) GSC-based adaptive beamformer with four taps per sensor, significant improvement in convergence speed and slight improvement in the steady-state signal-to-interference ratio (SINR) are observed in [5].

Traditionally, the design of FIBs is mainly focused on linear arrays with fixed spatial-frequency responses [4]–[7], [10], [11]. This is attributed to the attractive linear geometry of the array, which makes the design tractable and enables many efficient direction-of-arrival (DOA) estimation algorithms to be applied. For example, the MUSIC algorithm [12], which is a high-resolution method for detecting the angle of arrival (AoA) of the signal sources based on the subspace approach, has been proposed for uniform linear array to detect wideband coherent sources using

Manuscript received May 12, 2005; revised March 8, 2006. The associate editor coordinating the review of this manuscript and approving it for publication was Prof. Mats Viberg. Parts of this work are presented in the IEEE International Conference on Acoustics, Speech, and Signal Processing (ICASSP), Philadelphia, PA, March 18–23, 2005, and IEEE International Symposium on Circuits and Systems (ISCAS), Kobe, Japan, May 23–26, 2005.

The authors are with the Department of Electrical and Electronic Engineering, The University of Hong Kong, Hong Kong (e-mail: scchan@eee.hku.hk; hhchen@eee.hku.hk).

Color versions of Figs. 4, 6, 7, and 8 are available online at http://ieeexplore.ieee.org.

Digital Object Identifier 10.1109/TSP.2006.882109

FIBs [8]. Basically, MUSIC is applied to the beamspace generated by a set of fixed FIBs, with looking directions evenly distributed from -90° to 90° measured from the normal of the linear array. A related beamspace technique using discrete Fourier transform (DFT), called the frequency-domain FIBs, for wideband DOA estimation was also reported in [13].

Motivated by the potential advantages of FIB and the symmetric geometry of uniform circular arrays (UCA), Chan and Pun [14] developed an electronically steerable UCA in the digital domain with frequency-invariant (FI) characteristics and proposed to design the compensation filters using second-order cone programming (SOCP). Because of the circular symmetric geometry of UCAs, it was found that by transforming the snapshots to phase mode excitation or representation, the frequency dependency of the array can be equalized by a fixed beamforming network or the compensation filters. This gives rise to a FI array with its spatial response governed by a set of variable coefficients, one per each phase mode. This is very attractive because of the small number of adaptive weights required, which in turns yields faster convergence speed and fewer number of high-speed variable multipliers. The possibility of using compensation filters in UCA has recently been experimentally demonstrated for sonar applications in [15]. Unfortunately, the passband of a UCA is closely related to its radius and exhibit a bandpass characteristic (see Section III for details). In order to obtain a FI characteristic over a large bandwidth, the dynamic range of the coefficients in the compensation filters will become very large, and it leads to considerable noise amplification at the array output.

UCAs with FI characteristics have also been studied in the microwave communities [15]–[19]. The abovementioned problem of UCAs was observed in [19], where directional sensors with a broadband FI beampattern of $(1+\cos\phi)$ are employed. Here, ϕ is the azimuth angle of the array as shown in Fig. 3. The inclusion of the additional cosine term yields a final term with unity magnitude when the radius of the array is sufficiently large. Hence, the limitation of small phase mode coefficients on the bandwidth of the array can be alleviated.

In this paper, we proposed an alternative approach and show that this problem can also be mitigated if uniform concentric circular arrays (UCCAs) with ordinary omnidirectional sensors are employed. We find that UCAs with increasing radius will have their passbands being narrower (please refer to Section III and Appendix A for more details). Hence, by combining the outputs of ring subarrays with progressively larger radii in a UCCA, one can achieve a FI characteristic over a much larger bandwidth than a single UCA. Similar to the FI UCA in [14], snapshots of the proposed FI UCCA are transformed to the phase modes via inverse discrete Fourier transform (IDFT). The transformed data is then filtered to compensate for the frequency dependency of the phase modes. Unlike UCA, more nonzero contributions of phase mode are available from different rings. Therefore, more usable phase modes and a larger bandwidth can be achieved. After compensated for the frequency dependency of the phase modes by the compensation network, the data are then linearly combined using a set of weights or coefficients to obtain the desired FI beam patterns. These weights, which govern the far-field pattern of the UCCA, can be designed separately from the compensation network by conventional one-dimensional (1-D) digital filter design techniques such as the Parks–McClellan algorithm [20]. Alternatively, different beam patterns can be created by varying these coefficients in an adaptive beamformer with approximately FI characteristics. The compensation filters are designed using SOCP [21], [22] because of its optimality and ability to incorporate additional linear and convex quadratic constraints to the design problem. The compensation filter approach is also useful to the design of FI UCCA with fixed beampatterns because it significantly reduces the number of design parameters and hence the numerical difficulties by separately designing the beam weights and the compensation network.

Although the present approach may be more suitable to be implemented in acoustic applications, we would like to contrast its principle with the approach in [19], which is for microwave applications. First of all, the proposed approach requires only ordinary omnidirectional sensor elements, instead of specially designed broadband FI directional sensors. Second, the proposed system is based on optimization technique and it does not require the radius of the array be very large in order to achieve the desired frequency-invariance characteristic. In Appendix B, we also show that the beampattern in [19] can be realized using a two-ring UCCA. It is because this particular two-ring UCCA can be viewed as a structure to realize a special circular array with each sensor element having a characteristic of $(1+\cos\phi)$. Consequently, one gets a similar result in [19]. It should be noted that additional design freedom and implementation constraints may exist in realizing different types of sensing systems.

To demonstrate some of the potential benefits of the proposed UCCA-FIB, new broadband adaptive beamforming and DOA estimation algorithms using the UCCA-FIB are also developed in this paper. Thanks to the FI characteristic of the beamforming network, the variable beamforming weight of each phase mode can adapt as in a conventional narrowband adaptive beamformer. Therefore, conventional beamforming methods such as the minimum-variance beamforming (MVB) [23] and GSC [9] can be used to suppress the interference from the received data. Therefore, the length of the tapped-delay line can be drastically reduced (one per phase mode in our experiment). As a result, the arithmetic complexity associated with the adaptation of the lengthy tapped-delay lines in traditional broadband adaptive beamformers can be significantly reduced and the convergence speed, numerical property and output SINR can also be improved. Our DOA estimation algorithm is based on the method in [8], which was originally designed for ULA-FIB. In particular, narrowband DOA estimation algorithms, such as MUSIC, is applied to the beamspace generated by a set of fixed FI beamformers with looking directions evenly distributed from 0° to 360°, because of the FI characteristics of the FI UCCA arrays.

Several design examples on the design of UCCA-FIBs, the DOA estimation, and the adaptive beamforming using UCCA-FIBs are given. Design results show that electronic steerable beam patterns with approximately FI characteristic over a fairly large bandwidth can be obtained. The feasibility of the proposed adaptive beamforming and DOA estimation algorithms are verified by computer simulation using broadband multisinusoidal signals as well as Gaussian signals. Simulation results suggest that, compared with conventional broadband adaptive beamformers using the UCCA without the compensation fil-

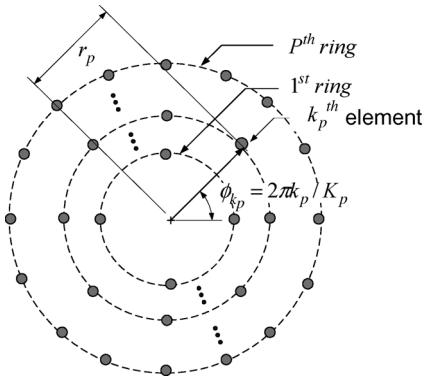

Fig. 1. UCCA with P rings. The pth ring has K_p equally spaced sensors.

ters, the proposed adaptive UCCA-FIB has better numerical property and output SINR due to the fewer number of adaptive beam weights and FI property. The proposed DOA and adaptive beamforming techniques are also applicable to FI UCAs, if a smaller bandwidth is acceptable.

The paper is organized as follows: In Sections II and III, the basic structure of the UCCA and the proposed digital broadband UCCA-FIB are presented. The design of the UCCA-FIBs using SOCP is described in Section IV. The proposed broadband DOA estimation and adaptive beamforming algorithms using the UCCA-FIB are presented in Sections V and VI, respectively. Design examples and simulation results are given in Section VII, and conclusions are drawn in Section VIII.

II. Uniform Concentric Circular Arrays (UCCAs)

Fig. 1 shows a UCCA with P rings and each ring has K_p omnidirectional sensors located at $\{r_p \cos\phi_{k_p}, r_p \sin\phi_{k_p}\}$ (represented as Cartesian Coordinate with the center as the origin) where r_p is the radius of the p^{th} ring, $p = 1, \cdots, P$, $\phi_{k_p} = 2\pi k_p / K_p$, and $k_p = 0, \cdots, K_p - 1$ as shown in Figs. 1 and 2. In UCCAs, the intersensor spacing in each ring is fixed at $\lambda/2$, where λ is the smallest wavelength of the array to be operated and is denoted by $\lambda_{\min}$. The radius of the p^{th} ring of the UCCA is given by

$$r_p = \lambda_{\min} / \left(4 \sin(\pi / K_p)\right). \tag{2.1}$$

For convenience, this radius is represented as its normalized version

$$\widetilde{r}_p = r_p / \lambda_{\min} = 1 / \left(4 \sin(\pi / K_p)\right). \tag{2.2}$$

Let α denote the ratio of the sampling frequency f_{s} to the maximum frequency $f_{\max}$ ($\alpha = f_s / f_{\max}$), the phase difference between the k_p^{th} sensor and the center of the UCCA is $\chi_{k_p} = 2\pi \widetilde{r}_p \alpha \sin\theta \cos(\phi - \phi_{k_p})$. For notation convenience, let

$$\hat{r} = \widetilde{r} \cdot \alpha \tag{2.3}$$

the corresponding frequency response of the phase difference can be expressed as $e^{j\omega \hat{r}_p \sin\theta \cos(\phi - \phi_{k_p})}$, where ω is the frequency variable, ϕ and θ are the azimuth angle and the elevation angle respectively, as shown in Fig. 3. The azimuth angle ϕ is

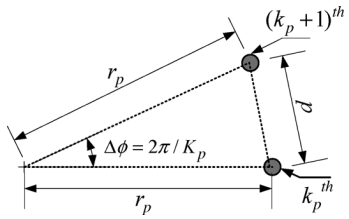

Fig. 2. Relationship between intersensor spacing and the radius of the pth ring of the UCCA.

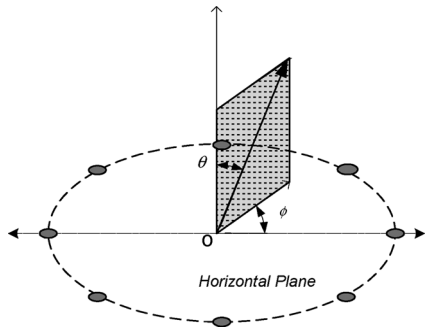

Fig. 3. Geometry of the reference imaginary frame.

on the horizontal plane where the sensors are situated. It measures from a reference imaginary axis on this horizontal plane, while the elevation angle θ is measured from a reference imaginary axis perpendicular to the horizontal plane. For a plane wave (i.e., far field) arriving at azimuth angle ϕ and elevation angle θ, the steering vector of the p^{th} ring of a UCCA is

$$\boldsymbol{a}_p(\omega, \phi) = \Big[e^{j\omega \hat{r}_p \sin\theta \cos(\phi - \phi_0)}, e^{j\omega \hat{r}_p \sin\theta \cos(\phi - \phi_1)}, \cdots, e^{j\omega \hat{r}_p \sin\theta \cos\left(\phi - \phi_{K_p - 1}\right)}\Big]^T. \tag{2.4}$$

Here, we shall focus our design at an elevation angle of $\theta = \pi/2$, i.e., the horizontal plane.

III. Digital Broadband UCCA-FIB

Fig. 4 shows the structure of the FI beamformer for a UCCA with P rings. After appropriate downconversion, lowpass filtering, and sampling, the sampled signals from the antennas of the p^{th} ring are given by the vector $\boldsymbol{x}_p[n] = [x_0^{(p)}[n] x_1^{(p)}[n] \cdots x_{K_p-1}^{(p)}[n]]^T$, which is called a snapshot at sampling instance n. This snapshot is IDFT to a set of Fourier coefficients, each coefficient is called a phase mode. The transformed snapshot is then denoted by $\boldsymbol{V}_p[n] = \boldsymbol{W}_{M_p, K_p} \cdot \boldsymbol{x}_p[n]$, where $\boldsymbol{W}_{M_p, K_p}$ is an $M_p \times K_p$ IDFT matrix with $[\boldsymbol{W}_{M_p, K_p}]_{m_p, k_p} = e^{j2\pi m_p k_p / K_p}$ and

$$[\boldsymbol{V}_p[n]]_{m_p} = v_{m_p}^{(p)}[n] = \sum_{k_p=0}^{K_p - 1} x_{k_p}^{(p)}[n] e^{j\frac{2\pi k_p m_p}{K_p}}. \tag{3.1}$$

Here, $[\boldsymbol{A}]_{m,n}$ denotes the $(\mathrm{m} \times \mathrm{n})$ entry of matrix $\boldsymbol{A}$. We assume that M_p is an odd number and define $L_p = (M_p - 1)/2$, $m_p = -L_p, \ldots, L_p$. Each branch of the IDFT output is then filtered by $H_{m_p}^{(p)}(\omega)$ (to compensate for the frequency dependency of the phase modes as we shall see later in this section), multiplied

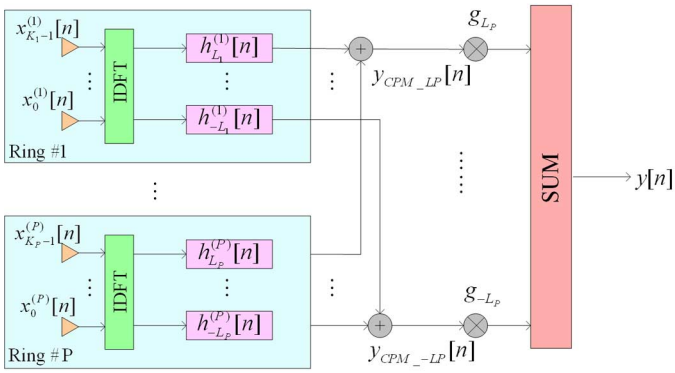

Fig. 4. UCCA-FIB block diagram.

with the variable beamformer weights $g_{m_p}^{(p)}$ before combining to give the beamformer output $y_p[n]$, as follows:

$$y_p[n] = \sum_{m_p=-L_p}^{L_p} \left(v_{m_p}^{(p)}[n] * h_{m_p}^{(p)}[n] \right) \cdot g_{m_p}^{(p)} \tag{3.2}$$

where $*$ denotes discrete-time convolution. To obtain the spatial–temporal transfer function of the beamformer, let us assume that there is only one source signal $s(n)$ with spectrum $S(\omega)$. Taking the discrete-time Fourier transform (DTFT) of (3.1), one gets

$$\begin{aligned} V_{m_p}^{(p)}(\omega) &= \sum_{k_p=0}^{K_p-1} X_{k_p}^{(p)}(\omega) e^{j\frac{2\pi k_p m_p}{K_p}} \\ &= S(\omega) \cdot \sum_{k_p=0}^{K_p-1} e^{j\omega \hat{r}_p \cos\left(\phi-\phi_{k_p}\right)} e^{j\frac{2\pi k_p m_p}{K_p}}. \end{aligned} \tag{3.3}$$

Taking DTFT on both size of (3.2) and using (3.3), we have

$$\begin{aligned} Y_p(\omega) &= \sum_{m_p=-L_p}^{L_p} g_{m_p}^{(p)} V_{m_p}^{(p)}(\omega) H_{m_p}^{(p)}(\omega) \\ &= S(\omega) \cdot \sum_{m_p=-L_p}^{L_p} g_{m_p}^{(p)} \\ &\quad \times \left(\sum_{k_p=0}^{K_p-1} e^{j\omega \hat{r}_p \cos\left(\phi-\phi_{k_p}\right)} e^{j\frac{2\pi k_p m_p}{K_p}} \right) H_{m_p}^{(p)}(\omega). \end{aligned} \tag{3.4}$$

Hence, the spatial–temporal response of the p^{th} ring of the UCCA is

$$\begin{aligned} G_p(\omega,\phi) &= \sum_{m_p=-L_p}^{L_p} g_{m_p}^{(p)} \\ &\quad \times \left[\sum_{k_p=0}^{K_p-1} e^{j\omega \hat{r}_p \cos\left(\phi-\phi_{k_p}\right)} e^{j\frac{2\pi k_p m_p}{K_p}} H_{m_p}^{(p)}(\omega) \right]. \end{aligned} \tag{3.5}$$

To obtain an FI response, the term inside the bracket, which is a function of both ϕ and ω, should be independent of the frequency variable ω. To this end, we make use of the Jacobi–Anger expansion [24]

$$e^{j\beta\cos\gamma} = \sum_{n=-\infty}^{+\infty} j^n J_n(\beta) e^{jn\gamma} \tag{3.6}$$

where $J_n(\beta)$ is the Bessel function of the first kind of order n, and rewrite (3.5) as

$$\begin{aligned} G_p(\omega,\phi) &= \sum_{m=-L_p}^{L_p} g_{m_p}^{(p)} \\ &\quad \times \left[\sum_{k_p=0}^{K_p-1} \sum_{n=-\infty}^{+\infty} j^n J_n(\omega \hat{r}_p) \right. \\ &\qquad \left. \times\, e^{jn(\phi-2\pi k_p/K_p)} e^{j\frac{2\pi k_p m_p}{K_p}} H_{m_p}^{(p)}(\omega) \right] \\ &= \sum_{m_p=-L_p}^{L_p} g_{m_p}^{(p)} \\ &\quad \times \left[\sum_{n=-\infty}^{+\infty} j^n J_n(\omega \hat{r}_p) e^{jn\phi} \right. \\ &\qquad \left. \times \left(\sum_{k_p=0}^{K_p-1} e^{j2\pi k_p\left(\frac{m_p-n}{K_p}\right)} \right) H_{m_p}^{(p)}(\omega) \right]. \end{aligned} \tag{3.7}$$

Further, the term inside the bracket is evaluated to be

$$\sum_{k_p=0}^{K_p-1} e^{j2\pi k_p\left(\frac{m_p-n}{K_p}\right)} = \begin{cases} K_p, & m_p - n = K_p q \\ 0, & \text{otherwise} \end{cases}, \text{ where } q \in \mathbb{Z}. \tag{3.8}$$

Substituting (3.8) into (3.7) gives

$$\begin{aligned} G_p(\omega,\phi) &= K_p \sum_{m=-L_p}^{L_p} g_{m_p}^{(p)} \\ &\quad \times \left[\sum_{n=m_p+K_p q} j^n J_n(\omega \hat{r}_p) e^{jn\phi} H_{m_p}^{(p)}(\omega) \right]. \end{aligned} \tag{3.9}$$

From [24], the Bessel function satisfies the following property:

$$\left| J_{|n|}(\omega \hat{r}_p) \right| \le \left(\frac{\omega \hat{r}_p e}{2|n|} \right)^{|n|}. \tag{3.10}$$

Therefore, for sufficiently large value of n, the value of the Bessel function will be negligibly small. In other words, if the number of sensors is large enough, we can truncate the infinite sum in (3.9) and retain the term with $n = m_p$ (i.e., $q = 0$). Consequently, $G_p(\omega,\phi)$ can be approximated by

$$G_p(\omega,\phi) \approx K_p \sum_{m_p=-L_p}^{L_p} g_{m_p}^{(p)} \left[j^{m_p} J_{m_p}(\omega \hat{r}_p) H_{m_p}^{(p)}(\omega) \right] \cdot e^{jm_p\phi}. \tag{3.11}$$

It can be seen that for a ring with given radius $\hat{r}_p$, the coefficient of the m_p^{th} phase mode before compensation is given by $J_{m_p}(\omega \hat{r}_p)$. Hence, the bandwidth is limited by the spacing of successive zeros of the Bessel function, which is fixed. Since

$J_{m_p}(u)$ decays as u increases, rings with larger radii will have a lower center frequency and bandwidth, while rings with smaller radii usually have better high frequency responses. A more detailed discussion is given in Appendix A. Therefore, to obtain an FI beamformer with large bandwidth using a UCA, small responses of $J_{m_p}(\omega\hat{r}_p)$ at certain frequencies have to be compensated by $H_{m_p}^{(p)}(\omega)$. This is undesirable in general because the dynamic range of the coefficients of $H_{m_p}^{(p)}(\omega)$ will increase rapidly with the signal bandwidth. Consequently, it may lead to considerable noise amplification in the array. Fortunately, by employing more rings in a UCCA, it will be shown below that $H_{m_p}^{(p)}(\omega)$ is required to compensate for a sum consisting of terms like $J_{m_p}(\omega\hat{r}_p)$, each coming from a phase mode of each ring. As mentioned earlier, rings with smaller radii have better high-frequency responses while rings with larger radii have better low-frequency responses. Therefore, by combining rings with appropriate radii, the response of the UCCA over the band of interest will not be vanishing small, although some of the phase mode coefficients with very small magnitude from certain rings will be discarded. As a result, the sum mentioned above, which is the frequency response of the array at different frequencies, will not be too small. Hence, it is possible to equalize this sum using numerical well-behaved compensation network $H_{m_p}^{(p)}(\omega)$'s and frequency invariance over a wider bandwidth can be achieved.

In a UCCA-FIB, the outer rings have more phase modes than the inner ones. For simplicity, we assume that the weighting vectors of the rings are identical, i.e., $g^{(p)} = g_m, p = 1, \ldots, P$. The overall response of the beamformer can be written as:

$$\begin{aligned} G(\omega,\phi) &= \sum_{p=1}^{P} G_p(\omega,\phi) \\ &= \sum_{m=-L_P}^{L_P} g_m \cdot e^{jm\phi} \\ &\quad \cdot \left[\sum_{p=1}^{P} K_p j^m J_m(\omega\hat{r}_p)\cdot H_m^{(p)}(\omega)\right]. \end{aligned} \quad (3.12)$$

From (3.12), it can be seen that if the filters $H_m^{(p)}(\omega)$ are designed in such a way that

$$\sum_{p=1}^{P} K_p j^m J_m(\omega\hat{r}_p)\cdot H_m^{(p)}(\omega) \approx 1 \text{ for } \omega \in [\omega_L,\omega_U], \quad m = -L_P,\ldots,L_P \quad (3.13)$$

where ω_L and ω_U are, respectively, the lower and upper frequencies of interest, then the beamformer in (3.12) will be approximately FI within $\omega \in [\omega_L,\omega_U]$ and

$$G(\omega,\phi) \approx \sum_{m=-L_P}^{L_P} g_m e^{jm\phi}. \quad (3.14)$$

Furthermore, the far-field beam pattern is now governed by the spatial weighting $\{g_m\}$ alone. For notational convenience, we shall just write $G(\phi)$ for the left-hand side of (3.14). It can also be seen from (3.14) that the far-field spatial response is similar to that of a digital FIR filter with impulse response $\{g_m\}$. Therefore, $G(\phi)$ can be designed by conventional filter design algorithms such as the Parks–McClellan algorithm [20] or SOCP [21] if convex quadratic constraints are to be imposed. Alternatively, real-time adaptation of the beam pattern through the spatial weighting $\{g_m\}$ can be employed to suppress undesired interference as will be seen in Section IV. To design the compensation network, we first notice that the left-hand side of (3.13) is a linear function of the filter coefficients in $H_m^{(p)}(\omega)$'s. Therefore, the design problem in (3.14) can be treated as a digital FIR filter design problem with all the filter outputs adding up to a desire response having a value of one. This will be discussed later in Section IV.

Before proceeding to the design of the compensation filters, we remark that there is usually mutual coupling between sensors in sensor arrays. It is beyond the scope of this paper to address further this problem for UCCAs. Interested readers are referred to [25] for more information of the mutual coupling effect of phase-mode-excited circular arrays and compensation method by modifying the amplitude and phase of each far-field phase mode pattern. The mutual coupling effect for narrowband UCA was also discussed in [26].

IV. Designing UCCA FIBs With SOCP

As mentioned in Section III, the problem of determining the filter coefficients of $H_m^{(p)}(\omega)$ can be formulated and solved using SOCP [21], [22]. SOCP is a convex programming problem and the global optimal solution is guaranteed if it exists. Another important advantage of SOCP is that it is very convenient to include additional linear or convex quadratic constraints, such as the norm constraints of the variable vector, to the design problem. It has been used in the optimal design of digital FIR filters and fixed beam broadband ULA FIBs [21]. A standard form of SOCP can be written as follows:

$$\begin{aligned} &\text{minimize } \boldsymbol{b}^T\boldsymbol{x} \\ &\text{subject to } \boldsymbol{d}_i^T\boldsymbol{x}+q_i \geq \|\boldsymbol{A}_i\boldsymbol{x}+\boldsymbol{c}_i\|_2,\ i=1,\ldots,N \end{aligned} \quad (4.1)$$

where $\boldsymbol{x} \in R^m$ is the variable vector; $\boldsymbol{b}$, $\boldsymbol{d}_i \in R^m$, $\boldsymbol{c}_i \in R^{n_i}$, and $q_i \in R$ are constant vectors; $\boldsymbol{A}_i \in R^{n_i\times m}$ are constant matrices; and $\|\boldsymbol{u}\|_2$ denotes the Euclidean norm of the vector $\boldsymbol{u}$. To begin with, let $h_m^{(p)}(n)$ be the coefficients of the compensation filter $H_m^{(p)}(\omega)$, i.e., $H_m^{(p)}(\omega) = \sum_{n=0}^{N_m^{(p)}} h_m^{(p)}[n]e^{-jn\omega}$. The approximation error is $E(\omega) = j^m \sum_{p=1}^{P} K_p J_m(\omega\hat{r}_p\alpha)(\sum_{n=0}^{N_m^{(p)}} h_m^{(p)}[n]e^{-jn\omega}) - 1$. If the minimax criterion is used, the design problem in (3.13) can be formulated as

$$\begin{aligned} &\text{mimimize } \delta \\ &\text{subject to } \|E(\omega)\|_2 = \left\| j^m \sum_{p=1}^{P} K_p J_m(\omega\hat{r}_p) \right. \\ &\qquad \left. \times \left(\sum_{n=0}^{N_m^{(p)}} h_m^{(p)}[n]e^{-jn\omega}\right) - 1 \right\|_2 \leq \delta, \\ &\qquad \omega \in [\omega_l,\omega_u] = \Omega,\ m = -L_P,\ldots,L_P \end{aligned} \quad (4.2)$$

where $N_m^{(p)}$ is the order of the filter $H_m^{(p)}$. Since $E(\omega)$ is a complex quantity, we need to evaluate its real and imaginary parts first. Because the value of j^m is dependent on m, we shall make

the substitution of variable $b_m^{(p)}[n] = j^m h_m^{(p)}[n]$ and solve the following problem in $b_{m_p}^{(p)}(n)$:

$$\begin{aligned}&\text{minimize } \delta\\ &\text{subject to } \left\|\sum_{p=1}^{P} K_p J_m(\omega\hat{r}_p)\left(\sum_{n=0}^{N_m^{(p)}} b_m^{(p)}[n]e^{-jn\omega}\right)-1\right\|_2 \le \delta,\\ &\qquad \omega\in\Omega,\ m=-L_P,\ldots,L_P. \end{aligned} \tag{4.3}$$

Using the identity $e^{-jn\omega} = \cos(n\omega) - j\sin(n\omega)$, (4.3) can be rewritten in a more compact matrix form as follows:

$$\begin{aligned}&\text{minimize } \delta\\ &\text{subject to } \left\|\sum_{p=1}^{P}\left[K_p J_m(\omega\hat{r}_p)\boldsymbol{c}_m^{(p)}(\omega)\boldsymbol{b}_m^{(p)}\right]-1-j\right.\\ &\qquad\left.\cdot\sum_{p=1}^{P} K_p J_m(\omega\hat{r}_p)\boldsymbol{s}_m^{(p)}(\omega)\boldsymbol{b}_m^{(p)}\right\|_2 \le \delta,\\ &\qquad \omega\in\Omega,\ m=-L_P,\ldots,L_P \end{aligned} \tag{4.4}$$

where $\boldsymbol{b}_m^{(p)} = [b_m^{(p)}(0),\ldots,b_m^{(p)}(N_m^{(p)})]^T$, $\boldsymbol{c}_m^{(p)}(\omega) = [1,\cos(\omega),\ldots,\cos(N_m^{(p)}\omega)]$, and $\boldsymbol{s}_{m_p}^{(p)}(\omega) = [0,\sin(\omega),\ldots,\sin(N_m^{(p)}\omega)]$. By stacking together δ and the coefficients of the P compensation filters $\boldsymbol{b}_m^{(p)}$'s into a vector $\boldsymbol{X}_m$, (4.4) can be rewritten in the following form:

$$\begin{aligned}&\text{minimize } \boldsymbol{d}^T\boldsymbol{X}_m\\ &\text{subject to } \|(\boldsymbol{C}_m(\omega)\boldsymbol{X}_m-1)-j\boldsymbol{S}_m(\omega)\boldsymbol{X}_m\|_2 \le \boldsymbol{d}^T\boldsymbol{X}_m,\\ &\qquad \omega\in\Omega,\ m=-L_P,\ldots,L_P \end{aligned} \tag{4.5}$$

where

$$\begin{aligned}\boldsymbol{d}^T &= [1,\ 0,\ \cdots,\ 0]\\ \boldsymbol{C}_m(\omega) &= \left[0,\ K_1J_m(\omega\hat{r}_1)\boldsymbol{c}_m^{(1)}(\omega),\ K_2J_m(\omega\hat{r}_2)\boldsymbol{c}_m^{(2)}(\omega),\right.\\ &\qquad\left.\cdots\ K_PJ_m(\omega\hat{r}_P)\boldsymbol{c}_m^{(P)}(\omega)\right]\\ \boldsymbol{S}_m(\omega) &= \left[0,\ K_1J_m(\omega\hat{r}_1)\boldsymbol{s}_m^{(1)}(\omega),\ K_2J_m(\omega\hat{r}_2)\boldsymbol{s}_m^{(2)}(\omega),\right.\\ &\qquad\left.\cdots\ K_PJ_m(\omega\hat{r}_P)\boldsymbol{s}_m^{(P)}(\omega)\right]\\ \boldsymbol{X}_m &= \left[\delta,\ \left(\boldsymbol{b}_m^{(1)}\right)^T,\ \left(\boldsymbol{b}_m^{(2)}\right)^T,\ \cdots,\ \left(\boldsymbol{b}_m^{(P)}\right)^T\right]^T.\end{aligned}$$

Finally, (4.5) can be written in a matrix form as follows:

$$\begin{aligned}&\text{minimize } \boldsymbol{d}^T\boldsymbol{X}_m\\ &\text{subject to } \boldsymbol{d}^T\boldsymbol{X}_m \ge \left\|\begin{pmatrix}\boldsymbol{C}_m(\omega)\\ \boldsymbol{S}_m(\omega)\end{pmatrix}\boldsymbol{X}_m+\begin{pmatrix}-1\\ 0\end{pmatrix}\right\|_2,\\ &\qquad \omega\in\Omega,\ m=-L_P,\ldots,L_P. \end{aligned} \tag{4.6}$$

By discretizing ω uniformly in Ω with sufficient number of points, say $K = 512$, each continuous constraint above for each m will yield K different constraints. The resulting problem is now in the form of a standard SOCP problem in (4.1), which can be solved efficiently using optimization toolbox such as SeDuMi [27].

It should be noted that the above two-stage method for designing separately the compensation filters and beam weights is also very useful to the design of fixed beam patterns with FI characteristics. Ideally, one can employ SOCP to design the compensation network and the beam weights jointly using (3.7), since it is also a linear function of the variables. However, we found that the number of variables and constraints for this direct approach is so large that both SOCP and semi-definite programming (SDP) solvers will encounter difficulties in convergence for arrays with only moderate number of elements and filter taps. On the other hand, the two-stage method decomposes the design problem into two independent problems of much smaller sizes. Consequently, it suffers from less numerical problem and consistently yields excellent results even with large number of elements and filter taps.

V. Broadband DOA Estimation Using UCCA-FIB

The UCCA-FIB designed in previous sections can be used in broadband DOA estimation. Following the method in [8], which is proposed for broadband DOA estimation using FI linear arrays, we use a set of UCCA-FIBs with fixed beampatterns and apply the MUSIC algorithm to its outputs to estimate the DOA's of the broadband sources. Consider I broadband signals impinging a P-ring UCCA at azimuth angles ϕ_i, $i = 1,\ldots,I$. The output signal at each element of the array can be written as

$$x_{k_p}^{(p)}[n] = \sum_{i=1}^{I} s_i\left[n-\tau_{k_p}(\theta_i)\right] + N_{k_p}^{(p)}[n], \tag{5.1}$$

where $s_i[n]$, $i = 1,\cdots,I$ are the arriving signals that impinge the array at angle ϕ_i, $i = 1,\cdots,I$. $N_{k_p}^{(p)}[n]$ is the additive white Gaussian sensor noise at the k_p^{th} element of the pth ring. As defined in Section III, the vector $\boldsymbol{x}_p[n] = [x_1^{(p)}[n],\cdots,x_{k_p}^{(p)}[n]]^T$ is called a snapshot at sampling instance n. The frequency response of the array output $\boldsymbol{x}_p[n]$ can be written as

$$X_p(\omega) = \boldsymbol{A}_p(\omega,\Phi)\boldsymbol{s}(\omega) + \boldsymbol{N}_p(\omega) \tag{5.2}$$

where $\boldsymbol{A}_p(\omega,\Phi) = [\boldsymbol{a}_p(\omega,\phi_1),\cdots,\boldsymbol{a}_p(\omega,\phi_I)]$ is the $K\times I$ source direction matrix for the pth ring, $\boldsymbol{a}_p(\omega,\phi_i)$, $i = 1,\cdots,I$, is the steering vector for the pth ring in (2.4), $\boldsymbol{s}(\omega) = [s_1(\omega),\cdots,s_I(\omega)]^T$ is the $I\times 1$ source signal vector and $\boldsymbol{N}_p(\omega) = [N_1^{(p)}(\omega),\cdots,N_{K_p}^{(p)}(\omega)]^T$ is the vector of the Gaussian noise at the sensors of the pth ring. After transforming to phase mode by IDFT, the outputs are

$$\boldsymbol{v}_p[n] = \boldsymbol{W}_p\boldsymbol{x}_p[n] \tag{5.3}$$

where

$$\boldsymbol{W}_p = \begin{pmatrix} 1 & e^{\frac{j2\pi\cdot(-L_p)}{K_p}} & e^{\frac{j2\pi\cdot 2\cdot(-L_p)}{K_p}} & \cdots & e^{\frac{j2\pi\cdot(K_p-1)\cdot(-L_p)}{K_p}}\\ \vdots & \vdots & \vdots & \cdots & \vdots\\ 1 & e^{\frac{j2\pi\cdot(-1)}{K_p}} & e^{\frac{j2\pi\cdot 2\cdot(-1)}{K_p}} & \cdots & e^{\frac{j2\pi\cdot(K_p-1)\cdot(-1)}{K_p}}\\ 1 & 1 & 1 & \cdots & 1\\ 1 & e^{\frac{j2\pi\cdot(1)}{K_p}} & e^{\frac{j2\pi\cdot 2\cdot(1)}{K_p}} & \cdots & e^{\frac{j2\pi\cdot(K_p-1)\cdot(1)}{K_p}}\\ \vdots & \vdots & \vdots & \cdots & \vdots\\ 1 & e^{\frac{j2\pi\cdot(L_p)}{K_p}} & e^{\frac{j2\pi\cdot 2\cdot(L_p)}{K_p}} & \cdots & e^{\frac{j2\pi\cdot(K_p-1)\cdot(L_p)}{K_p}} \end{pmatrix}.$$

Taking the DTFT of (5.3), the frequency response of the phase modes vector $\boldsymbol{v}_p[n]$ is given by

$$\boldsymbol{V}_p(\omega) = \boldsymbol{W}_p\boldsymbol{X}_p(\omega). \tag{5.4}$$

After passing through the compensation filters and the beam weights, the output of the pth ring of the beamformer is given by (3.2) and its frequency response is given by (3.4). In matrix form, (3.4) can be written as

$$\boldsymbol{Y}_p(\omega) = \boldsymbol{B}_p^H(\omega)\boldsymbol{V}_p(\omega) \tag{5.5}$$

where $\boldsymbol{Y}_p(\omega) = [Y_{-L_p}^{(p)}(\omega), \ldots, Y_{L_p}^{(p)}(\omega)]^T$ and $\boldsymbol{B}_p(\omega) = [g_{-L_p}H_{-L_p}^{(p)}(\omega), \cdots, g_{L_p}H_{L_p}^{(p)}(\omega)]^H$ is the $(M_p \times 1)$ beamformer vector. Using (5.2) and (5.4), the following frequency domain input–output relationship of the pth ring is obtained:

$$\boldsymbol{Y}_p(\omega) = \boldsymbol{B}_p^H(\omega)\boldsymbol{W}_p\boldsymbol{A}_p(\omega,\Phi)\boldsymbol{s}(\omega) + \boldsymbol{B}_p^H(\omega)\boldsymbol{W}_p\boldsymbol{N}_p(\omega). \tag{5.6}$$

From (3.3), (3.4) and (3.5), we can see that $\boldsymbol{B}_p^H(\omega)\boldsymbol{W}_p\boldsymbol{A}_p(\omega,\Phi) = \boldsymbol{G}_p(\omega,\Phi) = [G_p(\omega,\phi_1), \ldots, G_p(\omega,\phi_I)]^T$ and (5.6) becomes

$$\boldsymbol{Y}_p(\omega) = \boldsymbol{G}_p(\omega,\Phi)\boldsymbol{s}(\omega) + \boldsymbol{G}_p^{(N)}(\omega)\boldsymbol{N}_p(\omega) \tag{5.7}$$

where $\boldsymbol{G}_p^{(N)}(\omega) = \boldsymbol{B}_p^H(\omega)\boldsymbol{W}_p$. By adding the outputs of the P rings together, the overall frequency response of the beamformer is

$$\boldsymbol{Y}(\omega) = \sum_{p=1}^{P}\boldsymbol{Y}_p(\omega) = \boldsymbol{G}(\omega,\Phi)\boldsymbol{s}(\omega) + \boldsymbol{G}^{(N)}(\omega)\boldsymbol{N}(\omega). \tag{5.8}$$

where $\boldsymbol{G}(\omega,\Phi) = [\boldsymbol{G}(\omega,\phi_1), \cdots, \boldsymbol{G}(\omega,\phi_I)]$, $\boldsymbol{G}^{(N)}(\omega) = [\boldsymbol{G}_1^{(N)}(\omega), \cdots, \boldsymbol{G}_P^{(N)}(\omega)]$, $G(\omega,\phi_i) = \sum_{p=1}^{P} G_p(\omega,\phi_i)$, $i = 1, \ldots, I$, and $\boldsymbol{N}(\omega) = [\boldsymbol{N}_1(\omega), \cdots, \boldsymbol{N}_P(\omega)]^T$. To estimate the DOAs, we use J such beamformers to cover uniformly a given angular sector of interest $\Delta\phi$, where the sources are assumed to lie in. Denote the output of these J beamformers by $\boldsymbol{Y}_{\mathrm{FB\_1}}(\omega), \ldots, \boldsymbol{Y}_{\mathrm{FB\_}J}(\omega)$, and stack them together, one gets

$$\begin{aligned}\boldsymbol{Y}_{\mathrm{FB}}(\omega) &= [\boldsymbol{Y}_{\mathrm{FB\_1}}(\omega), \cdots, \boldsymbol{Y}_{\mathrm{FB\_}J}(\omega)]^T \\ &= \begin{pmatrix}\boldsymbol{G}_1(\omega,\Phi)\\ \vdots \\ \boldsymbol{G}_J(\omega,\Phi)\end{pmatrix}\boldsymbol{s}(\omega) + \begin{pmatrix}\boldsymbol{G}_1^{(N)}(\omega)\\ \vdots \\ \boldsymbol{G}_J^{(N)}(\omega)\end{pmatrix}\boldsymbol{N}(\omega) \\ &= \boldsymbol{G}_{\mathrm{FB}}(\omega,\Phi)\boldsymbol{s}(\omega) + \boldsymbol{G}_{\mathrm{FB}}^{(N)}(\omega,\Phi)\boldsymbol{N}(\omega)\end{aligned} \tag{5.9}$$

where $\boldsymbol{G}_i(\omega,\Phi)$ and $\boldsymbol{G}_i^{(N)}(\omega,\Phi)$ are respectively the gain of the signal and noise components in (5.8) for the ith beamformer. Since $\boldsymbol{G}(\omega,\Phi)$ has been designed to be approximately frequency invariant in the interested band, we have $\boldsymbol{G}_{\mathrm{FB}}(\omega,\Phi) \approx \boldsymbol{G}_{\mathrm{FB}}(\Phi)$, $\forall\omega \in [\omega_l, \omega_u]$. Assuming that the arriving signals and the noise are uncorrelated, the UCCA-FIBs data correlation matrix is given by

$$\begin{aligned}\boldsymbol{R}_y(\omega) &= E\left\{\boldsymbol{Y}_{\mathrm{FB}}(\omega)\boldsymbol{Y}_{\mathrm{FB}}^H(\omega)\right\} \\ &= \boldsymbol{G}_{\mathrm{FB}}(\Phi)\bar{\boldsymbol{R}}_s(\omega)\boldsymbol{G}_{\mathrm{FB}}^H(\Phi) \\ &\quad + \boldsymbol{G}_{\mathrm{FB}}^{(N)}(\Phi)\boldsymbol{R}_N(\omega)\left(\boldsymbol{G}_{\mathrm{FB}}^{(N)}(\Phi)\right)^H\end{aligned} \tag{5.10}$$

where $E\{\cdot\}$ is the expectation operator, the superscript H denotes the Hermitian transpose, and $\bar{\boldsymbol{R}}_s(\omega) = E\{\boldsymbol{s}(\omega)\boldsymbol{s}^H(\omega)\}$ and $\boldsymbol{R}_N(\omega) = E\{\boldsymbol{N}(\omega)\boldsymbol{N}^H(\omega)\}$ are the source and FIB noise correlation matrices. Integrating $\bar{\boldsymbol{R}}_y(\omega)$ over the frequency band of interest, we get the frequency-independent broadband FIB data correlation matrix

$$\begin{aligned}\boldsymbol{R}_y(\Phi) &= \int_{\Omega}\boldsymbol{R}_y(\omega)d\omega \\ &= \boldsymbol{G}_{\mathrm{FB}}(\Phi)\boldsymbol{R}_s\boldsymbol{G}_{\mathrm{FB}}^H(\Phi) + \boldsymbol{G}_{\mathrm{FB}}^{(N)}(\Phi)\boldsymbol{R}_N\left(\boldsymbol{G}_{\mathrm{FB}}^{(N)}(\Phi)\right)^H\end{aligned} \tag{5.11}$$

where $\boldsymbol{R}_s = \int_{\Omega}\boldsymbol{R}_s(\omega)d\omega$ and $\boldsymbol{R}_N = \int_{\Omega}\boldsymbol{R}_N(\omega)d\omega$ are the broadband FIB source and noise correlation matrices respectively. Denoting the IDFT of $\boldsymbol{Y}_{\mathrm{FB}}(\omega)$ as $\boldsymbol{y}_{\mathrm{FB}}(n)$ and using the Parseval's theorem, $\boldsymbol{R}_y(\Phi)$ can be computed from $y_{\mathrm{FB}}(n) = [y_{\mathrm{FB\_1}}(n), \cdots, y_{\mathrm{FB\_}J}(n)]^T$ as follows:

$$\begin{aligned}\boldsymbol{R}_y(\Phi) &= \int_{\Omega}\boldsymbol{R}_y(\omega)d\omega \approx \int_{-\pi}^{\pi}\boldsymbol{R}_y(\omega)d\omega \\ &= \sum_{n=-\infty}^{\infty}\boldsymbol{y}_{\mathrm{FB}}(n)\boldsymbol{y}_{\mathrm{FB}}^H(n).\end{aligned}$$

Here, we have assumed the out of band noise and signals have been appropriately filtered. The broadband FIB data covariance matrix $\boldsymbol{R}_y(\Phi)$, which contains the DOA information of the sources, can be used with conventional eigen-based DOA estimators such as MUSIC [12] to determine ϕ, the DOA.

Denote the eigendecomposition of $(\boldsymbol{R}_s, \boldsymbol{R}_N)$ as $\boldsymbol{R}_s\boldsymbol{E} = \boldsymbol{\Lambda}\boldsymbol{R}_N\boldsymbol{E}$, where $\boldsymbol{\Lambda}$ is a diagonal matrix of sorted eigenvalues and $\boldsymbol{E} = [\boldsymbol{E}_S|\boldsymbol{E}_N]$, where $\boldsymbol{E}_s$ and $\boldsymbol{E}_N$ are the eigenvectors of the signal and noise subspaces, respectively. The source directions can be determined by searching for the I peak positions of the following FIB-MUSIC spatial spectrum [8]:

$$\Theta(\phi) = \frac{\boldsymbol{G}(\phi)^H\boldsymbol{G}(\phi)}{\boldsymbol{G}(\phi)\boldsymbol{E}_N\boldsymbol{E}_N^H\boldsymbol{G}(\phi)}. \tag{5.12}$$

The J fixed beamformers, $G_1(\omega), \ldots, G_J(\omega)$ in (5.9), can be obtained by modulating the beamformer weight $\{g_m\}$ of a prototype beamformer focused at $\phi = 0$ with sinusoids at appropriate frequencies. For example, if the shift is $\pi/2$, then the modulation is $\{e^{j(\pi/2)m}\}$, $m = -L_P, \ldots, L_P$. The UCCA-FIB can also be used in adaptive beamforming to reconstruct the desired broadband signal and suppress the interference signals. Because of the FI characteristics of the beamformer, the length of the adaptive tapped-delay line can be largely reduced. Details of these adaptive UCCA-FIBs will be described next.

VI. Adaptive Beamforming Using UCCA-FIB

Consider I broadband signals impinging a P-ring UCCA at angles $\phi_1, \cdots$, and ϕ_I. The frequency response of the array is given by

$$Y(\omega) = \sum_{p=1}^{P}Y_p(\omega) \tag{6.1}$$

where $Y_p(\omega)$ is given by (3.4). Using (5.2), (5.4), and (3.4), $Y(\omega)$ can be rewritten as

$$Y(\omega) = \sum_{m=-L_P}^{L_P} g_m \cdot [\boldsymbol{a}_{G_m}(\omega, \Phi)\boldsymbol{s}(\omega) + N_m(\omega)] \qquad (6.2)$$

where $\boldsymbol{a}_{G_m}(\omega,\Phi)=\sum_{p=1}^{P} \boldsymbol{W}_m^{(p)} \boldsymbol{A}_p(\omega,\Phi) H_m^{(p)}(\omega)$, $N_m(\omega) = \sum_{p=1}^{P} \boldsymbol{W}_m^{(p)} H_m^{(p)}(\omega) N_m^{(p)}(\omega)$ and $\boldsymbol{W}_m^{(p)}$ is the m^{th} row of the transformation matrix $\boldsymbol{W}_p$. From Section III, we know that $\boldsymbol{a}_{G_m}(\omega,\Phi)$ is designed to be frequency invariant, and hence $\boldsymbol{a}_{G_m}(\omega,\Phi) \approx \boldsymbol{a}_{G_m}(\Phi)$, $\omega \in [\omega_l, \omega_u]$. Thus, the frequency response of the beamformer output is simplified to

$$Y(\omega) = \sum_{m=-L_P}^{L_P} g_m \left[\boldsymbol{a}_{G_m}(\Phi)\boldsymbol{s}(\omega) + N_m(\omega)\right]. \qquad (6.3)$$

Taking the IDFT, one gets the time-domain expression of the output as follows:

$$\begin{aligned} y[n] &= \sum_{m=-L_P}^{L_P} g_m \cdot [\boldsymbol{a}_{G_m}(\Phi)\boldsymbol{s}[n] + \eta_m[n]] \\ &= \sum_{m=-L_P}^{L_P} g_m y_{\text{CPM\_}m}[n], \end{aligned} \qquad (6.4)$$

where $g_m\eta_m[n]$, with Fourier transform (FT) $g_m N_m(\omega)$, is the output noise of the m^{th} phase mode of the beamformer, and $y_{\text{CPM\_}m}[n]$ is the m^{th} compensated phase mode. Equation (6.4) can also be written compactly in matrix form as follows:

$$y[n] = \boldsymbol{w}^H \boldsymbol{y}_{\text{CPM}}[n] = \boldsymbol{w}^H \boldsymbol{a}_G(\Phi) \cdot \boldsymbol{s}[n] + \boldsymbol{w}^H \boldsymbol{\eta}_{\text{CPM}}[n] \qquad (6.5)$$

where $\boldsymbol{w} = [g_1, \cdots, g_M]^H$, $\boldsymbol{a}_G(\Phi) = [\boldsymbol{a}_{G_{-L_P}}(\Phi), \cdots, \boldsymbol{a}_{G_{L_P}}(\Phi)]$ is an $(M \times I)$ source direction matrix with $\boldsymbol{a}_{G_m}(\omega,\Phi) \approx \boldsymbol{a}_{G_m}(\Phi)$ given by (6.2)

$$\boldsymbol{y}_{\text{CPM}}[n] = [y_{\text{CPM\_}-L_P}[n], \cdots, y_{\text{CPM\_}L_P}[n]]^T \qquad (6.6)$$

is the compensated phase mode vector, and $\boldsymbol{\eta}_{\text{CPM}}[n] = [\boldsymbol{\eta}_{\text{CPM\_}-LP}[n], \cdots, \eta_{\text{CPM\_}L_P}[n]]^T$ is the noise vector containing the noises at the compensated phase modes of the beamformer.

Assume that the desired signal impinges the array at an azimuth angle ϕ_d. To recover the desired signal from the array output, we employ the classical minimum variance beamformer (MVB) [23] (or minimum variance distortionless response MVDR beamformer). The basic idea of MVB is to choose the beamformer weight vector $\boldsymbol{w}$ such that the output energy of the array is minimized, while requiring the response of the array in the looking direction ϕ_d to be 1, hence the name MVDR. Mathematically, this means

$$\min_{\boldsymbol{w}} E\left[|y[n]|^2\right] \text{ with } \boldsymbol{w}^H \boldsymbol{a}_G(\phi_d) = 1$$

or, after using (6.5)

$$\begin{aligned} &\text{minimize } \boldsymbol{w}^H \boldsymbol{R}_{y\_\text{CPM}} \boldsymbol{w} \\ &\text{subject to } \boldsymbol{w}^H \boldsymbol{a}_G(\phi_d) = 1 \end{aligned} \qquad (6.7)$$

where $\boldsymbol{R}_{y\_\text{CPM}} = E\{\boldsymbol{y}_{\text{CPM}}[n] \cdot \boldsymbol{y}_{\text{CPM}}^H[n]\}$ is the autocorrelation of the compensated phase mode vector. This constrained optimization can be solved analytically and the optimal solution is

$$\boldsymbol{w}_{\text{opt}} = \frac{\boldsymbol{R}_{y\_\text{CPM}}^{-1} \boldsymbol{a}_G(\phi_d)}{\boldsymbol{a}_G(\phi_d)^H \boldsymbol{R}_{y\_\text{CPM}}^{-1} \boldsymbol{a}_G(\phi_d)}. \qquad (6.8)$$

Given a series of snapshots $\boldsymbol{y}_{\text{CPM}}[n]$, say $n = 1, \ldots, N$, the autocorrelation matrix can be estimated as $\hat{\boldsymbol{R}}_{y\_\text{CPM}} = \sum_{n=1}^{N} \boldsymbol{y}_{\text{CPM}}[n] \boldsymbol{y}_{\text{CPM}}^H[n]$. Thus, $\boldsymbol{w}_{\text{opt}}$ can be obtained by inverting the matrix $\hat{\boldsymbol{R}}_{y\_\text{CPM}}$ and substituting it into the right-hand side of (6.8). This is called the sample matrix inversion (SMI) method. Alternatively, $\boldsymbol{w}$ can be solved recursively using the adaptive filtering method such as the generalized sidelobe canceller (GSC) [28]. For simplicity and ease of comparison, the SMI method is used in this paper to assess the ultimate performance of the various approaches. Although the derivation above is based on one tap per phase mode, it can readily be generalized to include multiple taps as in traditional broadband beamformers, except that the input to the tapped-delay line, like the derivation above, is the compensated phase mode vector $\boldsymbol{y}_{\text{CPM}}[n]$.

We now roughly compare the arithmetic complexity of the adaptive beamformers using FI UCCA and the one employing tapped-delay line (TDL) UCCA. The arithmetic complexity of a digital beamformer usually consists of the complexities for the fixed filtering and the adaptive filtering parts. The order of the arithmetic complexity per sample for the fixed filtering part is usually linear in the filter length, while the order of arithmetic complexity per unit time for the adaptive filtering part will depend on the algorithm used. In this paper, the SMI algorithm is employed and the arithmetic complexity per second is of order $O(N^3)$, where N is the number of adaptive coefficients. Let T denote the length of the adaptive tapped-delay line and L_1 denote the length of the compensation filters in a FI UCCA, the complexity of the fixed and adaptive parts are, respectively, $O((\sum_{p=1}^{P} M_p) \times L_1)$ and $O((M_P \times T)^3)$, where M_p, $p = 1, \ldots P$, is the number of the usable phase modes of the p^{th} ring. In a TDL UCCA, broad band fractional delay digital filters are employed to steer the beam to the target direction. Let L_2 denote the length of these filters, the complexity of the fixed and adaptive filtering parts are respectively given by $O((\sum_{p=1}^{P} K_p) \times L_2)$ and $O((\sum_{p=1}^{P} K_p \times T)^3)$, where K_p, $p = 1, \ldots, P$, is the number of the sensors in the p^{th} ring. In the simulation of Example 3 to be presented in the next section, the numbers of sensors in the two rings of the UCCA are 10 and 18, respectively. The length of the compensation filters required is 31 and the number of usable phase modes is 9. On the other hand, the length of the broadband fractional delay filters in the TDL UCCA is 121. Therefore, the arithmetic complexity of this FI UCCA is $O(558) + O(729T^3)$, while that of a TDL UCCA is $O(3388) + O(21952T^3)$. It was found that the output SINR of the FI UCCA with $T = 1$ is better than that of the TDL UCCA with $T = 10$ for broadband Gaussian as well as multi-sinusoidal inputs tested. Therefore, the proposed FI UCCA is a good alternative to traditional TDL UCCAs because of its lower arithmetic complexity and higher output SINR. We now present

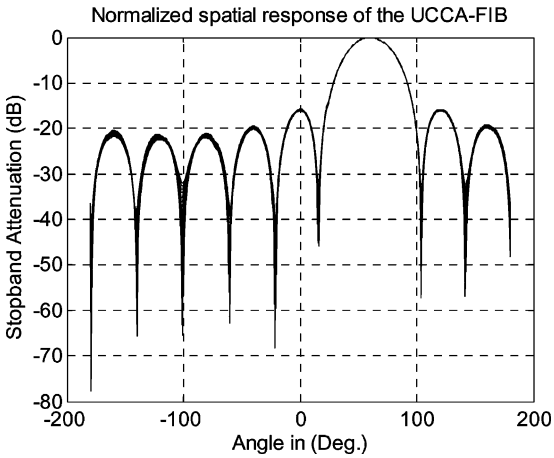

Fig. 5. Spatial response of the UCCA-FIB with two rings.

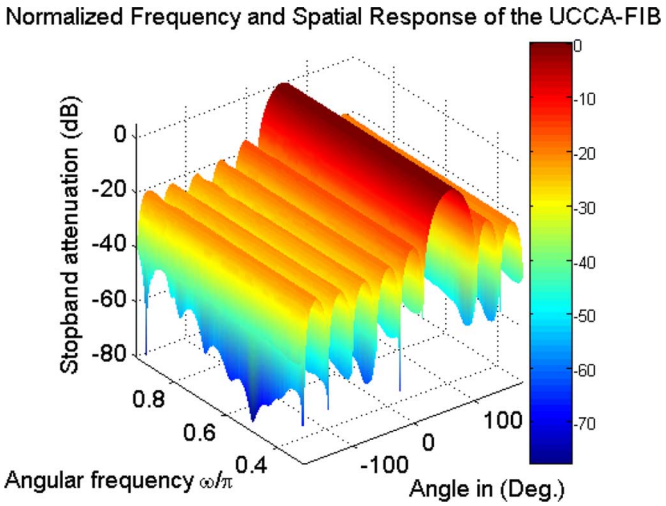

Fig. 6. Spatial–frequency response of the UCCA-FIB with two rings ($\omega \in [0.3\pi, 0.95\pi]$).

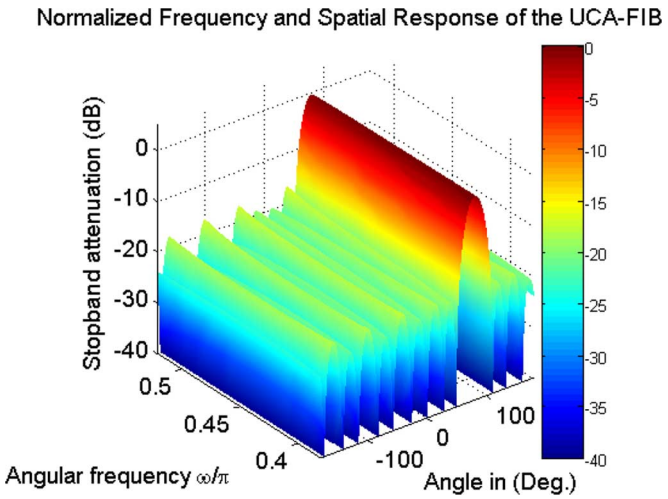

Fig. 7. Spatial–frequency response of the UCA-FIB ($\omega \in [0.38\pi, 0.52\pi]$).

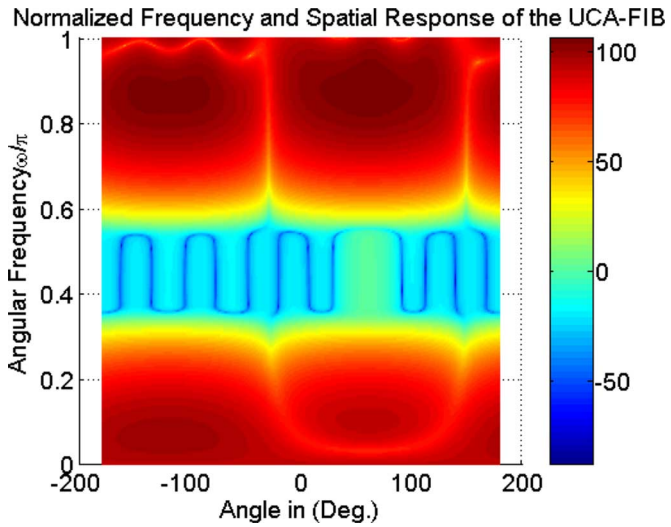

Fig. 8. Spatial–frequency response of the UCA-FIB in the entire band.

several design examples and simulation results to illustrate the principle of the proposed UCCA-FIB.

VII. Design Examples and Simulation Results

Example 1: UCCA-FIB With Two Rings: In this example, a two-ring UCCA is considered. The inner and the outer rings have respectively 10 and 18 omni-directional sensors. The required bandwidth of the UCCA-FIB is $\omega \in [0.3\pi, 0.95\pi]$. The numbers of phase modes M of the inner and outer rings are 9 and 17, respectively. The desired beam is targeted at 60°, and the beamwidth of the main lobe is 10°. The center 9 out of the 17 phase modes are chosen to avoid noise amplification, and the 9 spatial filter weights $\{g_m\}$ are obtained from the Parks–McClellan algorithm according to the direction and width of the desired beam. It was found experimentally that lower stopband attenuation at angles farther away from the passband usually gives a better DOA estimation result. Therefore, the following weightings [8, 1.6, 2.2, 1.2, 2.2, 1.6] are imposed respectively on successive spatial bands defined by the following angular intervals: [−180° −61°], [−60° −21°], [−20° 20°], [55° 65°], [95° 135°], [136° 180°]. These specifications are input to the CREMEZ command in Matlab, and the resultant frequency responses are shown in Figs. 5 and 6. For convenience, the frequency responses of the UCCA-FIB for $\omega \in [0.3\pi, 0.95\pi]$ are plotted together in Fig. 5 to illustrate the FI property of the beamformer. It can be seen that the frequency spectrum is approximately frequency invariant over the desired bandwidth. Fig. 6 shows the perspective view of the beamformer. As a comparison, Fig. 7 and Fig. 8 show respectively the perspective view of the spatial-frequency responses in the interested band and the entire frequency band for a UCA with 14 elements and 13 phase modes. We can see that the achievable frequency band is $[0.38\pi, 0.52\pi]$, which is much narrower than the UCCA, as explained in Section III and the Appendix A. The spatial–frequency responses of the UCA and UCCA outside the interested frequency bands are usually much higher than those in the interested bands. Therefore, appropriate bandpass filtering is required to remove these undesirable responses.

Example 2: UCCA-FIB With Three Rings: A three-ring UCCA will be considered. The numbers of sensors in each ring are 10, 18, and 28, respectively, and the desired bandwidth is

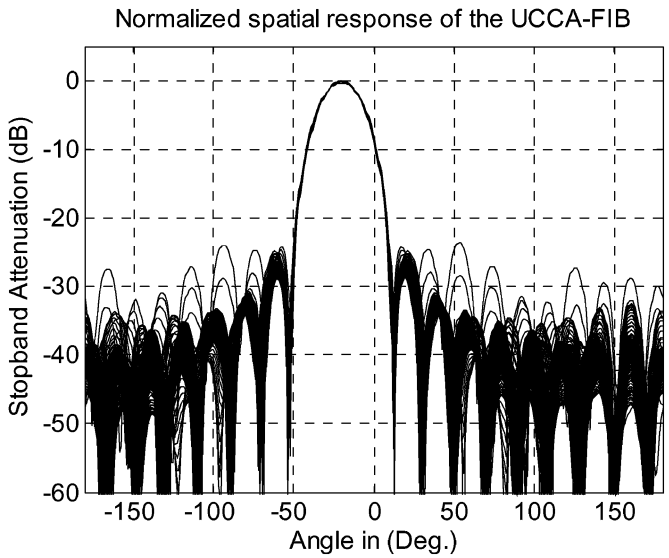

Fig. 9. Spatial response of the UCCA-FIB with three rings.

$\omega \in [0.3\pi, 0.95\pi]$. The numbers of phase mode M of the three rings are 9, 17, and 27, respectively, and the 17 phase modes out of the 27 are employed. The desired beam is targeted at -20°, and the beamwidth of the mainlobe is 10°. Again, the spatial filter weights $\{g_m\}$ with length 17 is designed using the Parks–McClellan algorithm according to the direction and width of the desired beam using CREMEZ command in Matlab with weightings [4 1.4 1.0 6 1.0 1.4 4] imposed on the following successive angular intervals: $[-180^\circ\ -86^\circ]$, $[-85^\circ\ -66^\circ]$, $[-65^\circ\ -50^\circ]$, $[-25^\circ\ -15^\circ]$, $[10^\circ\ 25^\circ]$, $[26^\circ\ 45^\circ]$, $[46^\circ\ 180^\circ]$. The frequency responses of the FIB so obtained in the range $\omega \in [0.3\pi, 0.95\pi]$ are shown in Fig. 9. Note that, the stopband attenuation is increased to 25 dB for the three-ring case because the number of usable phase modes and hence design freedom is increased.

Example 3: DOA Estimation Using the UCCA Beamformers: In this example, the performance of the proposed DOA estimation algorithm is evaluated using computer simulation of two broadband coherent signals at -35° and -40°. The first signal is composed of 33 sinusoidal signals with frequencies ranging from 0.8×10^8 to 4×10^8 Hz at an interval of 0.1×10^8 Hz. The other signal is a ten-sample delayed version of the first signal and the sampling rate constant α is set to 2. The prototype beamformer is a three-ring UCCA with 10, 26, and 36 elements in the first, second, and third rings, respectively. The other beamformers are obtained by shifting its response equally in the angular domain. The average SNR is 16.3 dB, and the number of arrays used in the beamspace is 5. The beamspace-MUSIC DOA estimation method proposed in Section V is employed. Fig. 10 shows the MUSIC spectrum in dB obtained and the estimated angles are found to be -34.97° and -40.06°, which are very close to the true values. Fig. 11 shows the root mean square error (RMSE) of estimating the DOA of a single broadband signal with different input SNRs. The result at each SNR is obtained by averaging 100 independent simulations. The performance of the UCCA-based DOA estimation algorithm is comparable to the one using linear array in [8]. The DOA estimation result (in RMSE) with two coherent Gaussian signals is comparable to the one using multicomponent sinusoidal signals above and it is omitted for space limitation.

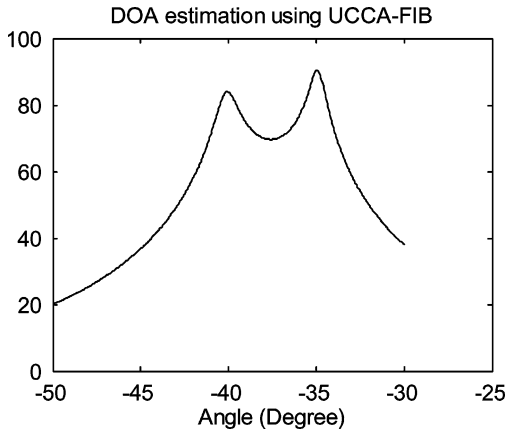

Fig. 10. DOA estimation of two coherent sources based on the three-ring UCCA-FIB.

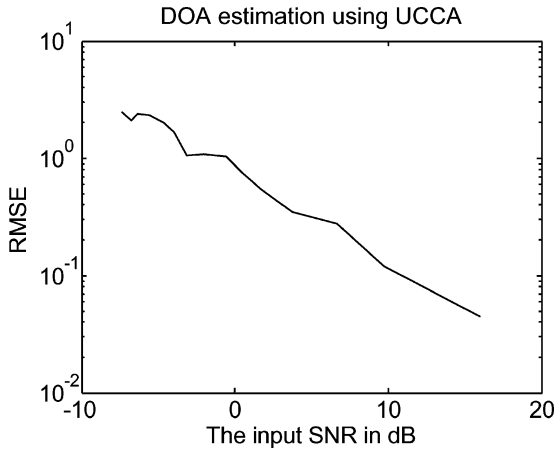

Fig. 11. Average RMSE of the DOA estimation for several SNR values.

Example 4: Adaptive Beamforming Using UCCA-FIB: In this example, the performance of the proposed adaptive UCCA-FIB is evaluated using computer simulation. The UCCA-FIB used is the same as the two-ring UCCA in the first example. The angles of arrival of the desired signal and the interfering signal are assumed to be 0° and 15°, respectively. Since the array can be electronically steered to the desired signal, the angle of arrival of the desired signal is simply assumed to be 0°. The desired signal is assumed to be composed of 53 sinusoidal signals with frequencies ranging from 0.8×10^8 to 6×10^8 Hz at an interval of 0.1×10^8 Hz. The interfering signal is also composed of 53 sinusoidal signals but with frequencies ranging from 0.83×10^8 to 6.3×10^8 Hz at an interval of 0.1×10^8 Hz. The additive sensor noises are assumed to be independent and identically distributed Gaussian random processes with zero means and same power. The input SNR and SIR are 16.67 dB and -20 dB, respectively. With the SMI beamforming method using UCCA-FIB described in Section VI, the desired signal is reconstructed using $N = 2 \times 10^4$ snapshots. The mean square error (MSE) between the output signal and the desired signal of the proposed UCCA-FIB versus

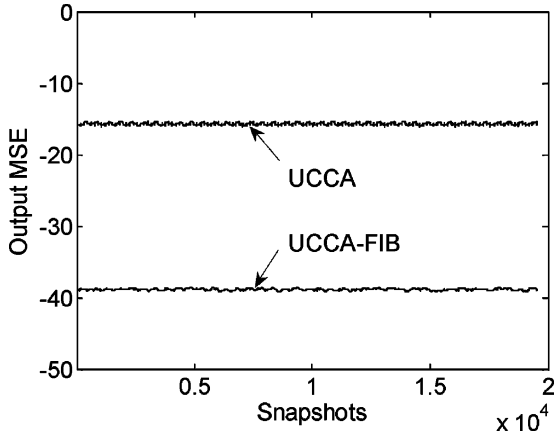

Fig. 12. Output MSE of the adaptive beamformers using UCCA and i) conventional tapped-delay line with one tap per sensor element (UCCA), ii) proposed FI adaptive beamformer with one tap per phase mode (UCCA-FIB).

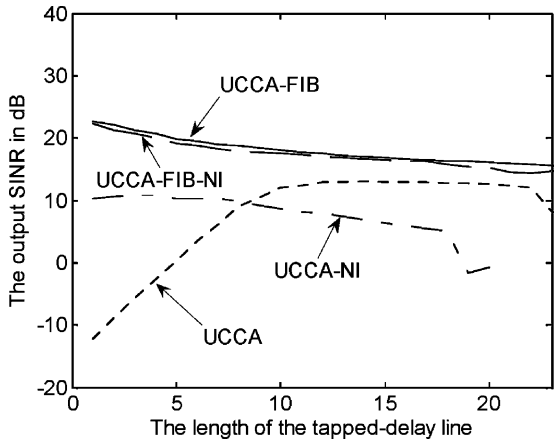

Fig. 13. Output SINRs versus tap length of the two adaptive beamformers using UCCA: i) conventional tapped-delay line in broadband (UCCA) and narrowband (UCCA-NI) interference, ii) proposed FI adaptive beamformer under broadband (UCCA-FIB) and narrowband (UCCA-FIB-NI) interference.

time is plotted in Fig. 12 as the line labeled UCCA-FIB. A broadband beamformer using the MVB principle and UCCA without the compensation network is also implemented and plotted in Fig. 12 as the line labeled UCCA for comparison. The simulation settings are identical to the UCCA-FIB and the length of the tapped-delay line is chosen as one to illustrate the effect of imposing the FI property. The MSE plot is obtained by averaging 100 independent trials, and it is further averaged across the snapshots with a window length of 300. From the simulation results, we can see that the reconstruction MSE of the SMI method using UCCA-FIB is -38 dB, which is 22 dB lower than that of the UCCA using a single coefficient, which is similar to a narrowband UCCA beamformer. The total number of adaptive coefficients in the UCCA-FIB is only 9.

We now evaluate the effect of varying the length of the tapped-delay line on the performance of the two adaptive beamforming methods: UCCA-FIB and conventional UCCA without the compensation filters. Fig. 13 shows the output SINR of the arrays versus different number of taps per sensor and phase mode in the UCCA and UCCA-FIB, respectively. The line labeled *UCCA-FIB* shows the beamforming result using UCCA-FIB, while the line labeled *UCCA* is for UCCA. The curves are obtained from averaging 100 independent trials. The x axis is the length of the tapped-delay line. From the figure, we can see that the performance of using one tap per phase mode in the UCCA-FIB is much better than that of the UCCA when the number of taps per sensor is less than 10. Since the number of sensor elements is 28, the total number of adaptive coefficients in the UCCA is 280 when the number of taps per sensor is 10. The performances of the UCCA-FIB and the conventional UCCA level off as the number of taps is further increased. The SINR of the conventional UCCA levels off when the number of taps is larger than 10, and it is slightly lower than that of the proposed UCCA-FIB. When the length is greater than 22, the number of adaptive coefficients in the UCCA is so large (more than 616) that its performance starts to degrade due to increased numerical errors. In other words, the proposed UCCA-FIB requires much fewer variable taps (a total of 9 when the number of tap per phase mode is one) than the UCCA and this in turns translates to lower complexity in adaptation, better numerical property and increased performance in output SINR. The output SINRs versus different numbers of adaptive tap for the UCCA and UCCA-FIB are also simulated with Gaussian input signals. The performances are comparable to the results of the multisinusoidal signal input case above. The SINRs are omitted due to page limitation.

Finally, we evaluate the performance of the two adaptive beamformers under strong narrowband interferences. The frequency of the interfering sinusoid signal is 3.03×10^8 Hz and the average SIR is -20 dB. The output SINRs versus the length of each tapped-delay line are plotted in Fig. 13. The performances of the UCCA and UCCA-FIB are plotted as lines labeled *UCCA-NI* and *UCCA-FIB-NI*, respectively. We can see from Fig. 13 that the performance of the proposed UCCA-FIB is not sensitive to NI, and it is almost identical to the broadband interference case with the same power. The performance of the conventional UCCA is much better than that in the broadband interference case, because a shorter tapped-delay line is able to annihilate the effect of a narrowband sinusoidal interference. When the length is increased beyond 5, the condition number of the system of linear equations becomes worse and the performance will degrade gradually. In all cases, it is at least 8 dB lower than that of the UCCA-FIB.

VIII. Conclusion

The theory and design of UCCAs having nearly FI characteristics are presented. By compensating the frequency dependency of individual phase modes using a digital beamforming network, the far-field pattern of the array is determined by a set of weights and it is approximately invariant over a wider range of frequencies than FI UCAs. New broadband DOA estimation and adaptive beamforming algorithms using the UCCA-FIB are also proposed. Simulation results using broadband multicomponent sinusoidal signals and Gaussian signals show that the proposed adaptive UCCA-FIB is numerically better conditioned than the conventional broadband tapped-delay-line-based adaptive beamformers, due to the FI property and significantly fewer numbers of adaptive parameters. The higher output SINRs achieved by the proposed

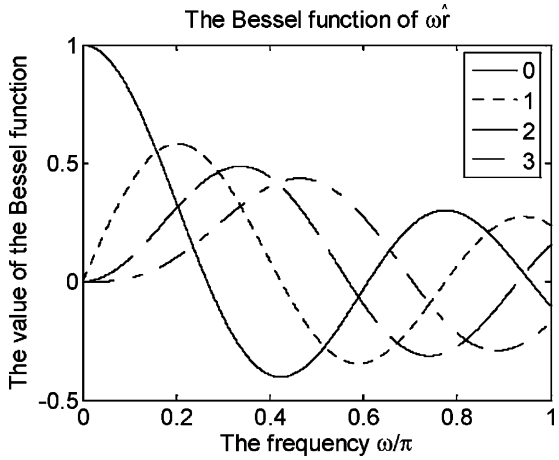

Fig. 14. Bessel function of UCA with normalized radius of 1.1235 ($K = 14$).

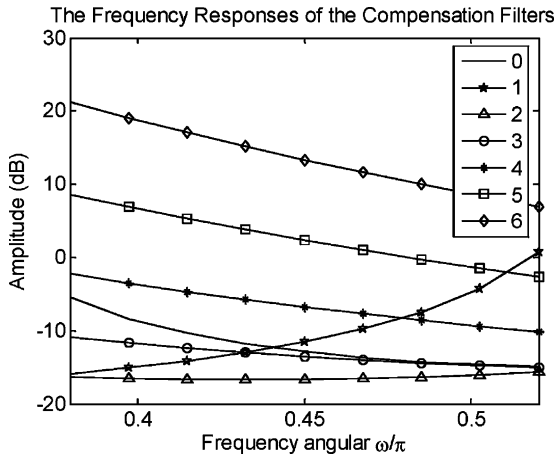

Fig. 15. Frequency responses of the compensation filters $H_m(\omega)$, $|m| = 0, \ldots, 6$, in Example 1.

approach also suggests that it is a good alternative to the conventional tapped-delay-line approach.

Appendix A
The Frequency Characteristics of Circular Arrays

Here, we examine the frequency response of a UCA. Consider a UCA with normalized radius $\widetilde{r} = 1.1235$, $\alpha = 2$, $K = 14$ and hence $\hat{r} = 2.247$. The Bessel function of $\omega\hat{r}$ is plotted in Fig. 14, where $\omega \in [0, \pi]$. The values of the zero- to third-order Bessel functions are plotted in the figure. For a UCA, $P = 1$ in (3.13), the compensation filter should be designed to satisfy the following equation to achieve frequency invariant:

$$H_m(\omega) = (Kj^m J_m(\omega\hat{r}))^{-1}, \quad \text{in the frequency band of interest.} \tag{A.1}$$

Obviously, the frequency band should not cover those frequencies where the values of the Bessel functions are zero. From Fig. 14, it can be seen that the possible frequency band is relatively narrow. Fig. 15 shows the frequency responses of the compensation filters designed in the UCA of Example 1. The dynamic range of the compensation filters for high order phase modes are relatively very large and they will amplify the additive noise. Therefore, these high-order phase modes should not be used in DOA estimation and beamforming. On the other hand, if the array has more than one ring, the frequency response of the entire UCCA is a combination of individual rings. Even if some of the rings have a small amplitude response, the other might not. As a result, if the radii of the ring are chosen appropriately, the compensation filter $H_m(\omega)$ will not assume large dynamic range and hence noise amplification. This is why UCCAs can achieve a larger bandwidth than UCAs. Higher stopband attenuation of the spatial responses of UCAs can also be obtained by employing more phase modes with a smaller sensor spacing of $(\lambda/4)$ [31]. However, this requires careful optimization of the ring radius and other circuit parameters. This additional freedom and design constraints, which may exist in different types of sensing systems such as microwave array systems, are not explored in this paper.

Generally speaking, the radii should be chosen according to the rule that at least one Bessel function value of a given phase mode coefficient in all the rings is not close to zero, say 10^{-3} or smaller, at the interested frequency band. In the UCCA of this paper, the distance between two adjacent sensors is fixed at $\lambda_{\min}/2$, so the relationship between the number of sensors in each ring and the radius is fixed. From our experiments, we find that satisfactory performance can be obtained if the difference of sensor numbers between two consecutive rings is set between 5 and 15.

Appendix B
Relationship Between the Directional Sensor Method and the Proposed FI UCCA

In this section, the relationship between the method in [19] using directional sensors and the proposed FI UCCA are described. According to (3.12), the m^{th} phase mode of the UCCA with two rings is

$$F_m(\phi) = e^{jm\phi} j^m \Big[K_1 J_m(\omega\hat{r}_1) H_m^{(1)}(\omega) + K_2 J_m(\omega\hat{r}_2) H_m^{(2)}(\omega)\Big] \tag{A.2}$$

where the coefficient g_m is omitted here for simplicity. If the two compensation filters are chosen as $H_m^{(1)}(\omega) = 1/K_1$ and $H_m^{(2)}(\omega) = j/2K_2[(J_{m+1}(\omega\hat{r}_1)/J_m(\omega\hat{r}_2)) - (J_{m-1}(\omega\hat{r}_1)/J_m(\omega\hat{r}_2))]$, the m^{th} phase mode can be written as

$$\begin{aligned} F_m(\phi) &= e^{jm\phi} j^m \left\{ K_1 J_m(\omega\hat{r}_1) \cdot \frac{1}{K_1} + K_2 J_m(\omega\hat{r}_2) \cdot \frac{j}{2K_2} \left[\frac{J_{m+1}(\omega\hat{r}_1)}{J_m(\omega\hat{r}_2)} - \frac{J_{m-1}(\omega\hat{r}_1)}{J_m(\omega\hat{r}_2)} \right] \right\} \\ &= e^{jm\phi} j^m \left\{ J_m(\omega\hat{r}_1) + \frac{j}{2} \times [J_{m+1}(\omega\hat{r}_1) - J_{m-1}(\omega\hat{r}_1)] \right\} \end{aligned} \tag{A.3}$$

which is the form of the UCA using directional sensors with a beampattern of $(1 + \cos\phi)$ proposed in [19]. With the UCCA structure, FI beamformers can be obtained using omnidirectional sensors. The reason for the above relationship is that

nearby omnidirectional sensors from the two rings and the compensation filters actually help to realize the required FI pattern in [19]. In addition, the radius of the circular array needs not to be very large.

ACKNOWLEDGMENT

The authors would like to thank the reviewers for their constructive comments, which greatly improve the presentation of the manuscript.

REFERENCES

[1] D. H. Johnson and D. E. Dudgeon, *Array Signal Processing: Concepts and Techniques*. Englewood Cliffs, NJ: Prentice-Hall, 1993.
[2] H. Krim and M. Viberg, "Two decades of array signal processing research: the parametric approach," *IEEE Signal Process. Mag.*, vol. 13, pp. 67–94, Jul. 1996.
[3] B. D. Van Veen and K. M. Buckley, "Beamforming: A versatile approach to spatial filtering," *IEEE Acoust., Speech, Signal Process. Mag.*, vol. 52, pp. 4–24, Apr. 1988.
[4] K. Nishikawa, T. Yamamoto, K. Oto, and T. Kanamori, "Wideband beamforming using fan filter," in *Proc. IEEE Int. Symp. Circuits Systems (ISCAS)*, 1992, vol. 2, pp. 533–536.
[5] T. Sekiguchi and Y. Karasawa, "Wideband beamspace adaptive array utilizing FIR Fan filters for multibeam forming," *IEEE Trans. Signal Process.*, vol. 48, no. 1, pp. 277–284, Jan. 2000.
[6] D. B. Ward, R. A. Kennedy, and R. C. Williamson, "Theory and design of broadband sensor arrays with frequency invariant far-field beam patterns," *J. Acoust. Soc. Amer.*, vol. 97, no. 2, pp. 1023–1034, Feb. 1995.
[7] ——, "FIR filter design for frequency invariant beamformers," *IEEE Signal Process. Lett.*, vol. 3, pp. 69–71, Mar. 1996.
[8] D. B. Ward, Z. Ding, and R. A. Kennedy, "Broadband DOA estimation using frequency invariant beamforming," *IEEE Trans. Signal Process.*, vol. 46, no. 5, pp. 1463–1469, May 1998.
[9] L. J. Griffiths and C. W. Jim, "An alternative approach to linearly constrained adaptive beamforming," *IEEE Trans. Antennas Propag.*, vol. AP-30, no. 1, Jan. 1982.
[10] J. O. Coleman and D. P. Scholnik, "Optimal design of wideband array patterns," in *Proc. IEEE RADAR 2000*, May 2000, pp. 172–177.
[11] M. Ghavami and R. Kohno, "Recursive fan filters for a broadband partially adaptive antenna," *IEEE Trans. Commun.*, vol. 48, pp. 185–188, Feb. 2000.
[12] R. O. Schmidt, "Multiple emitter location and signal parameter estimation," *IEEE Trans. Antennas Propag.*, vol. AP-34, pp. 276–280, Mar. 1986.
[13] T. Do-Hong, F. Demmel, and P. Russer, "A method for wideband direction-of-arrival estimation using frequency-domain frequency-invariant beamformers," in *Proc. IEEE Int. Symp. Antennas Propagation*, Jun. 2003, vol. 3, pp. 244–247.
[14] S. C. Chan and C. K. S. Pun, "On the design of digital broadband beamformer for uniform circular array with frequency invariant characteristics," in *Proc. IEEE Int. Symp. Circuits Systems (ISCAS)*, May 2002, vol. 1, pp. 693–696.
[15] Y. Yang, C. Sun, and C. Wan, "Theoretical and experimental studies on broadband constant beamwidth beamforming for circular arrays," in *Proc. IEEE OCEANS 2003*, Sep. 2003, vol. 3, pp. 1467–1653.
[16] H. Steyskal, "Circular array with frequency-invariant pattern," in *Dig. IEEE Int. Symp. Antennas Propagation*, 1989, vol. 3, pp. 1477–1480.
[17] D. E. N. Davies, "Circular arrays," in *The Handbook of Antenna Design*, A. W. Rudge, K. Milne, A. D. Olver, and P. Knight, Eds. Stevenage, U.K.: Peregrinus, 1983, vol. 11.
[18] M. R. Jones and H. D. Griffiths, "Prediction of circular array phase mode characteristics," *IEE Electron. Lett.*, vol. 24, no. 13, pp. 811–812, 1988.
[19] T. Rahim and D. E. N. Davies, "Effect of directional elements on the directional response of circular antenna arrays," *Proc. Inst. Elect. Eng., Part H: Microwaves, Optics, Antennas*, vol. 129, no. 1, pp. 18–22, Feb. 1982.
[20] T. W. Parks and J. H. McClellan, "Chebyshev approximation for nonrecursive digital filters with linear phase," *IEEE Trans. Circuits Syst.*, vol. 19, no. 2, pp. 189–194, Mar. 1972.
[21] J. O. Coleman and D. P. Scholnik, "Design of nonlinear phase FIR Filters with second-order cone programming," in *Proc. IEEE Midwest Symp. Circuits and Systems (MWSCAS)*, 1999, vol. 1, pp. 409–412.
[22] M. S. Lobo, L. Vandenberghe, S. Boyd, and H. Lebret, "Applications of second-order cone programming," *Linear Algebra Appl.*, vol. 248, pp. 193–228, Nov. 1998.
[23] J. Capon, "High-resolution frequency-wavenumber spectrum analysis," *Proc. IEEE*, vol. 57, no. 8, pp. 1408–1418, Aug. 1969.
[24] M. Abramowitz and I. A. Stegun, *Handbook of Mathematical Functions*. New York: Dover, 1965.
[25] I. D. Longstaff, P. E. K. Chow, and D. E. N. Davies, "Directional properties of circular arrays," *Proc. Inst. Elect. Eng.*, vol. 114, no. 6, pp. 713–718, 1967.
[26] M. Wax and J. Sheinvald, "Direction finding of coherent signals via spatial smoothing for uniform circular arrays," *IEEE Trans. Antennas Propag.*, vol. 42, no. 5, pp. 613–620, May 1994.
[27] J. F. Sturm, "Using SeDuMi 1.02, a MATLAB toolbox for optimization over symmetric cones," *Optim. Meth. Softw.*, vol. 11–12, pp. 625–653, 1999.
[28] K. M. Buckley and L. J. Griffiths, "An adaptive generalized sidelobe canceller with derivative constraints," *IEEE Trans. Antennas Propag.*, vol. AP-34, no. 3, pp. 311–319, Mar. 1986.
[29] S. C. Chan and H. H. Chen, "Theory and design of uniform concentric circular arrays with frequency invariant characteristics," in *Proc. IEEE Int. Conf. Acoustics, Speech, Signal Processing (ICASSP)*, Mar. 2005, vol. 4, pp. 805–808.
[30] ——, "Adaptive beamforming using Uniform Concentric Circular Arrays with frequency invariant characteristics," in *Proc. IEEE Int. Symp. Circuits Systems (ISCAS)*, May 2005, vol. 5, pp. 4321–4324.
[31] M. R. Jones and H. D. Griffiths, "Broadband pattern synthesis from a circular array antennas and propagation," in *Proc. Int. Conf. Antennas and Propagation (ICAP) 1989*, 1989, vol. 1, pp. 55–59.

S. C. Chan (S'87–M'92) received the B.Sc. (Eng.) and Ph.D. degrees from the University of Hong Kong in 1986 and 1992, respectively.

In 1990, he joined the City Polytechnic of Hong Kong as an Assistant Lecturer and later as a University Lecturer. Since 1994, he has been with the Department of Electrical and Electronic Engineering, the University of Hong Kong, where he is currently an Associate Professor. He was a Visiting Researcher at Microsoft Corporation, Redmond, WA, in 1998 and at Microsoft China in 1999. His research interests include fast transform algorithms, filter design and realization, multirate signal processing, communications signal processing, and image-based rendering.

Dr. Chan is currently a member of the Digital Signal Processing Technical Committee of the IEEE Circuits and Systems Society. He was Chairman of the IEEE Hong Kong Chapter of Signal Processing from 2000 to 2002.

H. H. Chen (S'06) received the B.Sc. and M.Eng. degrees in electrical and electronic engineering from Nankai University, Tianjin, China, in 1995 and 1999, respectively. She is currently working towards the Ph.D. degree at the Department of Electrical and Electronic Engineering in The University of Hong Kong, Hong Kong.

Her current research interests include digital signal processing, broadband sensor arrays, and their applications.